Improvement of EUV Spectra by Optical Thickness Control*)

Tsukasa SUGIURA[1)], Masaki KUME[1)], Hiroki MORITA[1)], Shinichi NAMBA[2)] and Takeshi HIGASHIGUCHI[1)]

[1)]*Department of Electrical and Electronic Engineering, Utsunomiya University, Utsunomiya 321-8585, Japan*
[2)]*Department of Advanced Science and Engineering, Hiroshima University, Higashihiroshima 739-8527, Japan*

(Received 15 July 2024 / Accepted 16 September 2024)

In double pulse cross-laser irradiation configuration, we measured the extreme ultraviolet (EUV) spectral purity and emission energy around 6.x nm wavelength in laser produced Gd plasmas. It was found that the spectral purity of 4.1% within a 0.6% bandwidth ($\Delta\lambda$ = 6.74 - 6.78 nm) at 6.76 nm to the total emission between wavelengths of 5 - 9 nm was improved by producing a low-density Gd plasma target, compared to the spectral purity of 1.6% for solid-Gd target plasma. A low-density plasma must be produced before the main heating laser pulse to enhance the spectral purity. We also reported the delay time dependence of the spectral purity irradiated by the 6-ns, 1-μm main laser pulse irradiation under the cross-laser-injection scheme.

Keywords: extreme ultraviolet (EUV), beyond EUV (B-EUV), gadolinium (Gd), highly charged ion (HCI)

DOI: 10.1585/pfr.20.2406004

1. Introduction

Extreme ultraviolet (EUV) lithography for semiconductor high-volume manufacturing (HVM) is a critical industrial technology [1]. The source in the EUV exposure tool is based on a laser-produced plasma formed on a tin (Sn) droplet that emits strongly in the 13.5-nm spectral region [2]. An unresolved transition array (UTA) emission due to $n = 4$ to $n = 4$ transitions emitted from highly charged open 4d subshell Sn ions is an essential optical transition for 13.5-nm wavelength. A higher numerical-aperture (NA) optical system and a higher power EUV source are indispensable if greater resolution is to be obtained on the silicon substrate in the exposure tool. According to the recent “International Roadmap for Devices and Systems (IRDS^{TM}),” the next technologies will require a higher NA of 0.55 or operate at a shorter EUV wavelength, so-called beyond EUV (B-EUV) with a wavelength of 6.x nm [3].

Potential B-EUV sources have been studied to investigate their spectral structure and conversion efficiency (CE). Note that the CE is defined as the ratio of in-band B-EUV emission energy to incident laser energy. The CEs reported were typically 0.3% - 0.4%, and the spectral purity (SP) or spectral efficiency, defined as the ratio of the emission within a 0.6% bandwidth ($\Delta\lambda$ = 6.74 - 6.78 nm) at 6.76 nm to the total emission between wavelengths of 5 - 9 nm was 2.4% at a main laser wavelength of 1 μm (Nd:YAG laser) [4, 5]. On the other hand, the CE and SP were 1.2% and 4.3%, respectively, at a main laser wavelength of 10.6 μm (CO_2 laser) [6, 7]. The SP for a lower critical density plasma produced at a laser wavelength of 10.6 μm is thus higher than that of a denser plasma produced at a laser wavelength of 1 μm due to small optical thickness for the EUV wavelength.

The bandwidth (BW) of the collector (C_1) mirror for B-EUV emission around 6.x nm is narrower than that for the 13.5-nm EUV Mo/Si multilayer mirror with a BW of 2%. High-power EUV sources are instrumental in enhancing in-band emission and suppressing out-of-band emission, thereby increasing the SP. This is crucial to avoid thermal effects, optical distortion, and critical dimension errors caused by out-of-band emission. The three main factors that determine CE are the absorption rate of the laser energy by the plasma, the CE to radiation, including EUV emission, and the SP. Therefore, we should tune the peak wavelength at 6.x nm and the emission spectrum bandwidth with high SP.

In the solid-state 1-μm laser-produced rare-earth element plasmas, such as the Gd and Tb plasmas, the spectral bandwidths are broader than that of the 10-μm laser-produced plasmas [6, 7]. Therefore, controlling the critical density related to the optical thickness is of significance. Under optically thin conditions by the pre-plasma production, the spectral bandwidth at a peak wavelength of 6.76 nm, which was attributed to the Gd^{18+} ions, was narrower when the 1-μm laser pulse was irradiated. We have achieved the narrow bandwidth emission spectrum using the solid-state laser-produced Gd plasma by means of the double pulse irradiation scheme [8]. The highest SP was 5.1% for the sub-ns (150-ps), 1-μm main laser pulse irradiation. However, there is no spectral behavior of the delay time dependence between the 16-ns, 1-μm pre laser pulse and the 6-ns, 1-μm main laser pulse under the cross-laser-

author's e-mail: higashi@cc.utsunomiya-u.ac.jp

*) This article is based on the presentation at the 26th International Conference on Spectral Line Shapes (ICSLS2024).

injection configuration. Compared to the sub-nanosecond main laser, the nanosecond main laser's plasma is optically thicker, potentially causing self-absorption that affects the spectral response. For instance, the spectral dip at 6.76 nm in Gd plasmas has been linked to optical thickness [9]. The cross-laser-injection configuration with the 1-µm main laser pulse enables us to investigate the cause of this dip. In this paper, we generate the spectral dip at 6.76 nm in the Gd plasma under the cross-laser-injection configuration. We also report on the dependence of the SP and emission energy on time separation between the 16-ns, 1 µm pre-pulse and the 6-ns, 1-µm main laser pulse irradiations.

2. Experimental Condition

Figure 1 shows a schematic diagram of the experimental setup under the cross-laser-injection configuration. Two Q-switched Nd:yttrium-aluminum-garnet (Nd:YAG) lasers operating at a wavelength of 1064 nm for the pre-pulse and main pulse were employed. The two laser systems were synchronized using a pulse delay oscillator (Stanford Research Systems Inc., DG645) with a jitter of less than one ns. The pre-plasma was generated on the edge of a planar Gd target with a width of 1 mm.

The intensity of the 16-ns pre-pulse was 4.5×10^8 W/cm^2 and a loose focal spot diameter of 2.5 mm. The beam was loosely focused to produce a large volume of pre-formed plasma (pre-plasma). The pre-pulse irradiated the target at normal incidence and at 90° to the main laser axis. The main laser irradiated the pre-plasma at a distance between z = 70 - 500 µm above the target surface at a delay time of $\Delta\tau$ = 10 - 200 ns after the pre-pulse laser irradiation. The main laser intensity was kept at 2.4×10^{12} W/cm^2 with a pulse duration of 6 ns. The transmittance was measured by the energy meter in Fig. 1. The transmittance was defined the ratio between the transmitted laser pulse energy through the pre-plasma and the incident laser pulse energy.

The B-EUV emission spectra were measured by a flat-field grazing incidence spectrometer with an unequally ruled 2400 grooves/mm grating. The spectrometer was positioned at 30° with respect to the incident main laser axis. Time-integrated B-EUV spectra were recorded by a thermoelectrically cooled back-illuminated x-ray charge-coupled device (CCD) camera (Andor Technology Inc.). The typical spectral resolution was better than 0.01 nm [10]. The pressure inside the vacuum chamber was kept at 1×10^{-4} Pa.

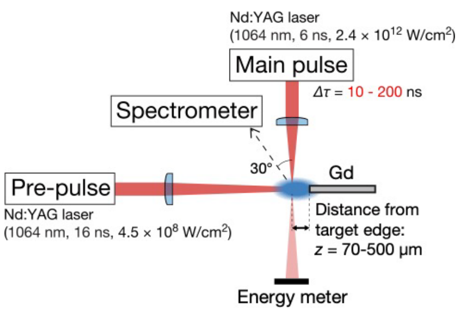

Fig. 1 Schematic diagram of the experimental setup.

3. Experimental Results and Discussion

3.1 Spectral comparison at different optical thickness conditions

We compared the time-integrated B-EUV spectra under optically thick and thin plasma conditions. We produced optically thick condition by the 1-µm laser pulse irradiation to the planar solid Gd target (red line) in Fig. 2. The main laser pulse intensity was 2.4×10^{12} W/cm^2. The critical density was 1×10^{21} cm^{-3}, and the effective B-EUV emission region was expected to be originated from the expanding plasma surface at the electron density of the order of 10^{19} cm^{-3} [11]. The observed spectrum was broader, attributed to the multiple highly charged Gd ions, with a dip at a wavelength of 6.76 nm. The SP was 1.6%. On the other hand, we observed the narrow spectrum (SP = 3.9%) under optically thin conditions produced by the pre-formed Gd plasma (pre-plasma) at a main focal position of z = 70 µm and the delay time of $\Delta\tau$ = 20 ns (see the red line in Fig. 2). The spectral peak under optically thin condition (blue line) was in good agreement with the spectral dip under optically thick (red line). We believe that the dip at 6.76 nm appeared due to the self-absorption process (weak opacity effect) of the B-EUV emission by the dense Gd plasma. We need the numerical calculation of the radiation hydrodynamic simulation with the atomic process in plasmas [2].

3.2 B-EUV emission spectra and SP behaviors

Figure 3 shows the peak-intensity-normalized time-integrated B-EUV spectra at different delay times of $\Delta\tau$ = 20 - 60 ns at z = 70 µm in Fig. 1. The peak wavelength

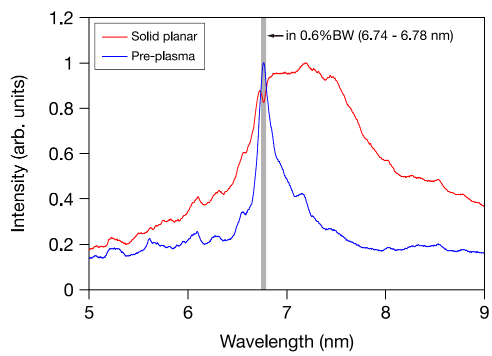

Fig. 2 Spectral comparison for the optically thick (red) and optically thin (blue) conditions.

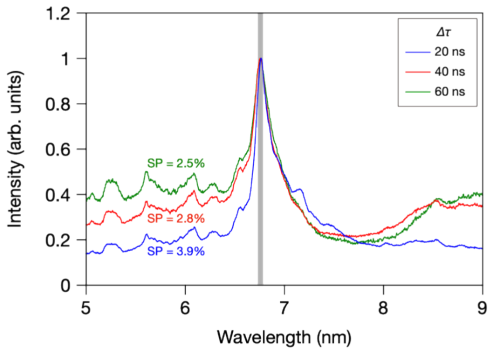

Fig. 3 The normalized time-integrated B-EUV spectra at three different delay times of $\Delta\tau$ = 20 - 60 ns at z = 70 µm.

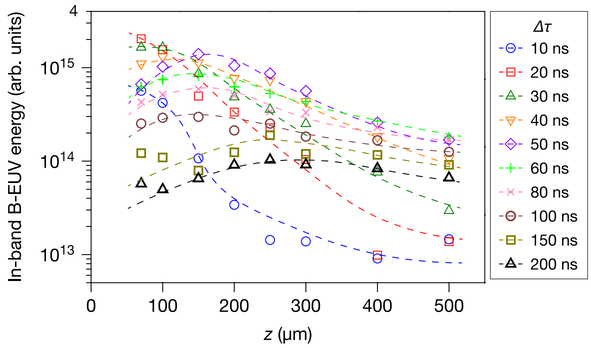

Fig. 5 Dependence of in-band B-EUV energy on distance from target at each delay time.

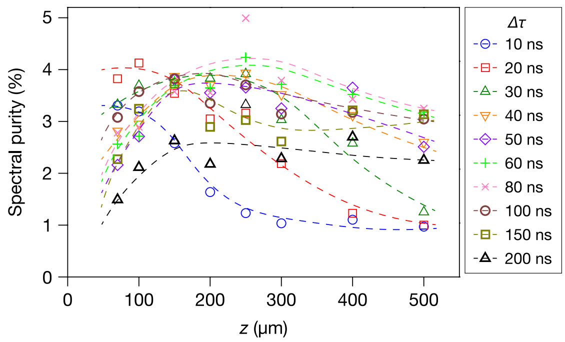

Fig. 4 Dependence of spectral purity on distance from the target at each delay time.

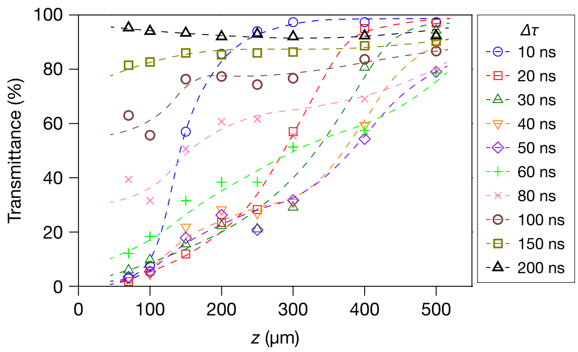

Fig. 6 Dependence of transmittance of the main laser pulse on distance from the target at each delay time.

remains at 6.76 nm. Note that the gray band corresponds to the reflection bandwidth of 0.6% of the multilayer mirror for the 6.x-nm B-EUV emission in Fig. 3. The SPs are 3.9% at $\Delta\tau$ = 20 ns, 2.8% at $\Delta\tau$ = 40 ns, and 2.5% at $\Delta\tau$ = 60 ns.

It is important to understand the spectral behavior, which is coupled with the narrow reflection bandwidth of the multilayer collector mirror. Under the optically thin pre-plasma condition imposed, this peak, which is mainly due to the $4d^{10}\ ^1S_0 - 4d^9 4f^1 P_1$ [$n = 4 - n = 4$ ($\Delta n = 0$)] transition of Pd-like Gd^{18+} overlapped with $^2F - ^2D$ lines of Ag-like Gd^{17+} near 6.76 nm [12, 13]. A similar structure has also been observed in a discharge-produced plasma [12], which, like CO_2-laser-produced Gd plasmas [6, 7], is optically thin due to its relatively low critical density of 1×10^{19} cm^{-3}. Note that the spectral features shorter than 6.76 nm originate from higher than Gd^{19+} and arise from $n = 4 - n = 5$ transitions.

We plotted the spatiotemporal SP behavior in Fig. 4, and the corresponding in-band B-EUV emission energy is shown in Fig. 5. The maximum SP was 4.1% at the delay time of 20 ns and the main laser pulse focal position of 100 µm, as shown in Fig. 4. The in-band B-EUV emission is almost maximized at the delay time of $\Delta\tau$ = 20 ns and the spatial region of z = 50 - 100 µm, as plotted in Fig. 5. In addition, we show the transmittance of the main laser pulse in Fig. 6. The transmittance laser was measured to be about 5% at the delay time of $\Delta\tau$ = 20 ns and the spatial region of z = 50 - 100 µm in Fig. 6.

Past delays of $\Delta\tau$ = 20 - 60 ns, the longer wavelength emission decreased with the increase of the time delay due to successively lower plasma densities resulting from pre-plasma expansion. At shorter delays, the plasma emission was reduced either as a consequence of reduced plasma size or increased opacity in the smaller, denser plasma volume. A simple plasma expansion can explain the SP behavior of the delay time dependence. The time taken for the density of the pre-plasma expanding at sound velocity to decrease to its critical density for maximum absorption of the main laser pulse was evaluated to be in 50 ns, which almost agrees well with the observed optimum delay time of $\Delta\tau$ = 20 - 60 ns, under the present set of experimental parameters with an evaluated sound velocity of 8×10^2 cm/s at the present pre-pulse laser intensity and an estimated electron temperature of 6 eV. Subsequently, the effective number of Gd ions emitting the 6.7-nm B-EUV emission decreased with increasing scale length of the density and temperature gradients as the time separation increased.

In detail, there are two different conditions to maximize the SP and the in-band B-EUV emission at the delay time of $\Delta\tau$ = 20 ns and the spatial region of z = 50 - 100 µm and at the delay time of $\Delta\tau$ = 50 ns and the spatial region of z = 100 - 150 μm. The transmittances of the main laser pulse are T = 5% - 20%. This means that the laser absorption in pre-plasma is more significant. The present scheme can dramatically improve the SP, effectively coupled with the narrow-in-band multilayer B-EUV mirror. To optimize the condition for an efficient B-EUV source, we again need a more detailed numerical calculation of the radiation hydrodynamic simulation with the atomic process code in plasmas [2].

4. Summary

In summary, we have described the B-EUV spectral purity and emission energy of Gd laser plasma under the cross-laser-injection configuration. The spectral dip at 6.76 nm in the Gd plasma was observed. We believe that the reason why the dip at 6.76 nm had appeared was by the self-absorption process (weak opacity effect) of the B-EUV emission by the dense Gd plasma. The spectral purity of 4.1% was maximized by producing a low-density Gd plasma target, compared to the spectral purity of 1.6% for solid-Gd target plasma. The maximum SP was 4.1% at the delay time of 20 ns and the main laser pulse focal position of 100 μm. In near future, we will run the numerical simulation to understand the spectral behavior of the laser-produced plasma B-EUV source.

Acknowledgments

The authors are indebted to Takeru Niinuma and Hayato Yazawa (Utsunomiya University) for useful technical support and discussion. T.H. acknowledges the support from the Japan Society for the Promotion of Science (JSPS) / INTERNATIONAL JOINT RESEARCH PROGRAM and The Sumitomo Foundation.

[1] I. Fomenkov *et al*., Adv. Opt. Technol. **6**, 173 (2017).
[2] A. Sunahara *et al*., Opt. Express **31**, 31780 (2023); and references therein.
[3] IEEE, see https://irds.ieee.org/editions/2022/executive-summary for "Executive Summary: 2022 Edition of the International Roadmap for Devices and Systems (IRDS)" (2022).
[4] T. Higashiguchi *et al*., Appl. Phys. Lett. **99**, 191502 (2011).
[5] T. Cummins *et al*., Appl. Phys. Lett. **100**, 061118 (2012).
[6] T. Higashiguchi *et al*., Opt. Express **21**, 31837 (2013).
[7] R. Amano *et al*., Jpn. J. Appl. Phys., Part 1 **57**, 070311 (2018).
[8] M. Kume *et al*., Appl. Phys. Lett. **124**, 052107 (2024).
[9] H. Ohashi *et al*., J. Appl. Phys. **115**, 033302 (2014).
[10] T.-H. Dinh *et al*., Rev. Sci. Instrum. **87**, 123106 (2016).
[11] K. Yoshida *et al*., Appl. Phys. Lett. **106**, 121109 (2015).
[12] B. Li *et al*., Appl. Phys. Lett. **99**, 231502 (2011).
[13] B. Li *et al*., Appl. Phys. Lett. **101**, 013112 (2012).